Published in final edited form as:
Glia. 2013 September ; 61(9): 1500–1517. doi:10.1002/glia.22537.

Modulation of Rho-ROCK Signaling Pathway Protects Oligodendrocytes Against Cytokine Toxicity via PPAR-α-Dependent Mechanism

Ajaib S. Paintlia[#1], **Manjeet K. Paintlia**[#1], **Avtar K. Singh**[2], and **Inderjit Singh**[1]

[1]Department of Pediatrics, Darby Children's Research Institute, Medical University of South Carolina, South Carolina

[2] Department of Pathology and Laboratory Medicine, Ralph H. Johnson VA Medical Center, Charleston, South Carolina.

[#] These authors contributed equally to this work.

Abstract

We earlier documented that lovastatin (LOV)-mediated inhibition of small Rho GTPases activity protects vulnerable oligodendrocytes (OLs) in mixed glial cell cultures stimulated with Th1 cytokines and in a murine model of multiple sclerosis (MS). However, the precise mechanism of OL protection remains unclear. We here employed genetic and biochemical approaches to elucidate the underlying mechanism that protects LOV treated OLs from Th1 (tumor necrosis factor-α) and Th17 (interleukin-17) cytokines toxicity in *in vitro*. Cytokines enhanced the reactive oxygen species (ROS) generation and mitochondrial membrane depolarization with corresponding lowering of glutathione (reduced) level in OLs and that were reverted by LOV. In addition, the expression of ROS detoxifying enzymes (catalase and superoxide-dismutase 2) and the transactivation of peroxisome proliferators-activated receptor (PPAR)-α/-β/-γ including PPAR-γ coactivator-1α were enhanced by LOV in similarly treated OLs. Interestingly, LOV-mediated inhibition of small Rho GTPases, i.e., RhoA and cdc42, and Rho-associated kinase (ROCK) activity enhanced the levels of PPAR ligands in OLs via extracellular signal regulated kinase (1/2)/p38 mitogen-activated protein kinase/cytoplasmic phospholipase 2/cyclooxygenase-2 signaling cascade activation. Small hairpin RNA transfection-based studies established that LOV mainly enhances PPAR-α and less so of PPAR-β and PPAR-γ transactivation that enhances ROS detoxifying defense in OLs. In support of this, the observed LOV-mediated protection was lacking in PPAR-α-deficient OLs exposed to cytokines. Collectively, these data provide unprecedented evidence that LOV-mediated inhibition of the Rho–ROCK signaling pathway boosts ROS detoxifying defense in OLs via PPAR-α-dependent mechanism that has implication in neurodegenerative disorders including MS.

Keywords

lovastatin; EAE/MS; oligodendrocyte progenitors; PPAR-α; RhoA-ROCK; survival; differentiation

Correspondence to: Inderjit Singh, Department of Pediatrics, Medical University of South Carolina, 173 Ashley Avenue, Charleston, South Carolina 29425. singhi@musc.edu.

Introduction

Growing evidence suggests that oligodendrocyte (OL) health is crucial for neuronal axon survival under various neurodegenerative disorders including multiple sclerosis (MS) (Funfschilling et al., 2012; Oluich et al., 2012). Cytokines secreted by myelin reactive $CD4^+$ Th1 and Th17 cells play a critical role in the pathogenesis of experimental autoimmune encephalomyelitis (EAE), the murine model of MS (Brosnan and Raine, 1996; Gocke et al., 2007). Accumulating evidence suggests that proinflammatory cytokines largely affect OLs in MS brain (Oluich et al., 2012; Soulika et al., 2009). Th1 cytokines, i.e., tumor necrosis factor (TNF)-α and interferon-γ, enhance the generation of reactive oxygen species (ROS) in OLs leading to their apoptotic cell death in *in vitro* (Andrews et al., 1998; Pang et al., 2005). In line with this, we earlier documented that TNF-α reduces cellular glutathione level and enhances ceramide generation in OLs that eventually contribute to their apoptotic cell death (Singh et al., 1998). In addition, we recently documented that synergy between TNF-α- and Th17 cytokine-, interleukin-17 (IL-17), induced signaling mechanisms exacerbate the apoptotic cell death of OLs in *in vitro* (Paintlia et al., 2011). These findings indicate that the understanding of molecular mechanism(s) that protects OLs from Th1/Th17 cytokine holds promise for search of better therapeutics for MS and related neurodegenerative disorders.

Statins as cholesterol lowering drugs are documented to provide anti-inflammatory and neuroprotective activities in EAE and in *in vitro* culture systems (Paintlia et al., 2005; Youssef et al., 2002) and decline the gadolinium-enhancing MRI lesions in MS brain (Vollmer et al., 2004). Statin-mediated inhibition of small Rho GTPases activity reduces inflammatory components (myelin reactive $CD4^+$ Th1 and Th17 cells), endothelial dysfunction, and CNS inflammation in the EAE model (Dunn et al., 2006; Floris et al., 2004; Greenwood et al., 2003). Importantly, small Rho GTPases and peroxisome proliferator-activated receptors (PPARs) activities are reported to exhibit an inverse relationship in statin-treated cells (Yano et al., 2007). For instance, statin-mediated inhibition of RhoA activity increases PPAR-γ transactivation in immune cells that, in turn, modulate their pathogenicity under pathological conditions (Shen et al., 2010; Yano et al., 2007). We and others earlier reported that statin-mediated inhibition of RhoA activity enhances the differentiation of OL progenitor cells (OPCs) into myelin-forming OLs via PPAR-γ activation (Miron et al., 2007; Paintlia et al., 2010; Sim et al., 2008).

PPARs are a group of nuclear receptor proteins that function as transcription factors to regulate the expression of key genes involved in the cellular lipid metabolism (Amri et al., 1995; Forman et al., 1995). In addition, PPARs play a significant role in the development and differentiation of OPCs (Saluja et al., 2001; Woods et al., 2003). Moreover, PPAR agonists are reported to diminish clinical symptoms in the EAE model (Dunn et al., 2010; Klotz et al., 2009). In light of this information, we asked whether statin-mediated regulation of PPARs activity protects OLs from Th1/Th17 cytokine toxicity in the EAE/MS brain. To address this, we employed genetic and biochemical approaches in primary OLs and B12 cells (OL cell line) exposed to Th1 (TNF-α) and Th17 (IL-17) cytokines in the presence or absence of lovastatin (LOV) in *in vitro* settings. Our findings demonstrated that LOV-mediated inhibition of Rho family GTPases and Rho-associated kinase (ROCK) activity increases ROS detoxifying defense in OLs exposed to cytokines via PPAR-α-dependent mechanism.

Materials and Methods

Chemicals and Reagents

Dulbecco's modified eagle's medium (DMEM; containing 4.5 g/L glucose), fetal bovine serum (FBS), and poly-D-lysine (PDL; 50 μg/mL) including rat and rabbit polyclonal IgGs,

Alexa Fluor conjugated with anti-rabbit IgG or anti-mouse IgG, and/or phalloidin were from Life Technologies (Grass Island, NY). Recombinant platelet derived growth factor-aa (PDGF-aa), basic fibroblast growth factor-2 (bFGF-2), ciliary neurotrophic factor (CNTF), TNF-α, and IL-17 proteins including anti-myelin basic protein (MBP), anti-galactocerebroside (GalC), and anti-neuronal cell surface antigen (A2B5) antibodies were from Santa Cruz Biotechnology (Santa Cruz, CA). Anti-A2B5 MicroBeads and MS columns were from MACS, Miltenyi Biotec (Auburn, CA). Lovastatin (LOV), Y27632, WY14643, GW6471, ciglitazone, GW9662, L-165041, cyclooxygenase-2 (COX-2) inhibitor 1, arachidonyl trifluoromethyl ketone, and SB203580 were from EMD4Biosciences (Savannah, GA). Antibodies against PPAR-α/-β/-γ, phosphorylated extracellular-regulated-receptor-kinase (ERK) 1/2, phosphorylated p38 MAPK, PPAR-γcoactivator-1α (PGC-1α), catalase, manganese superoxide dismutase (SOD2), and CREB binding protein (CBP) were from Affinity BioReagents (Golden, CO). Antibodies against RhoA, cdc42, Rac1, and phosphocytoplasmic phospholipase 2 (cPLA2) were from Cell Signaling Technology (Danvers, MA).

Cultures and Treatments of OLs

Pregnant Sprague-Dawley rats were purchased from Harlan Laboratories (Dublin, VA) and the pregnant wild-type and PPAR-$\alpha^{(-/-)}$ mice was generated by breeding of their colonies. Pups were euthanized by decapitation in accordance with the protocol approved by the Medical University of South Carolina Institutional Animal Care and Use Committee as per the National Institute of Health Guide for the Care and Use of Laboratory Animals. The dissociated cortices were cultured in DMEM as described earlier (Paintlia et al., 2013). De-attached OPCs obtained from mixed glial cultures after shaking were incubated with anti-A2B5 MicroBeads for 1 h and passed through MS columns (MACS, Miltenyi Biotec) that showed >99.9% purity of OPCs (FACS analysis). OPCs (2,000 cells/cm^2) were plated in PDL-coated culture dishes or glass cover slips in serum-free modified Bottenstein–Sato-based medium (Bottenstein and Sato, 1979) supplemented with trophic factors, i.e., PDGF-aa and basic FGF (10 ng/mL each) as described earlier (Paintlia et al., 2010). After 24 h, fresh Sato-based medium supplemented with CNTF (10 ng/mL) was replaced in cells and further incubated for 48 h which showed the transformation of OPCs into OL-lineages, i.e., O4$^+$ (50% ± 5%), O1$^+$ and O1$^+$/MBP$^+$ (35% ± 2%), and MBP$^+$ (15% ± 1%) as analyzed by FACS analysis. For treatment studies; OLs were cultured in Sato-based medium supplemented with 2% FBS and exposed to TNF-α (10 ng/mL) and IL-17 (25 ng/mL). OLs were treated with LOV (2.0 μM) or other pharmacological agents for 2 h prior to cytokine exposure. B12 cells were a kind gift from David Schubert (Salk Institute, La Jolla, CA), which are rat OL cell lines that express O1, CNPase, and MBP (Roth et al., 2003). B12 cells were preferred for transfection studies over primary OLs due to their better transfection efficiency. B12 cells (2,000 cells/cm^2) were cultured in DMEM containing 5% FBS and 25 μg/mL gentamycin (Nunc, Roskilde, Denmark) and incubated at 37° C in a humidified atmosphere of 95% air and 5% CO_2 (Calderon et al., 1998). Seventy to eighty percent confluence cultures of B12 cells were transfected with plasmids and used for experimental studies. Concentrations of the pharmacological agents or LOV used in the study demonstrated no cell death as measured by trypan blue exclusion and LDH release assays.

ROS Measurements

Cellular ROS levels were measured using cell-permeable fluorescent dye 5-(and-6)-chloromethyl-2′,7′-dichlorodihydrofluorescein diacetate (CM-DCFDA; Invitrogen) as described previously (Paintlia et al., 2011). For positive control, cells were treated with 0.3% H_2O_2 in culture media and incubated for 30 min at 37° C (data not shown). Data were plotted as percentage of controls.

Glutathione Measurements

The concentration of glutathione (GSH) (reduced) in cells was measured immediately after homogenization in lysis buffer using a Glutathione assay kit (Biotium, Hayward, CA). This kit is based on monochlorobimane that forms a fluorescent conjugate with GSH as described earlier (Keelan et al., 2001). Samples were read after 30 min at 380/460 nm using a Soft Max Pro spectrofluorometer (Molecular Devices, Sunnyvale, CA). Cells treated with staurosporine (1 micro gram/mL) were used as positive control (data not shown). Changes in GSH levels are expressed as nmol/mg of cellular protein.

Mitochondrial Membrane Potential (Δ Ψ m) Measurements

Changes in ΔΨm were measured in treated cells using JC-1 (5,5′,6,6′-tetrachloro-1,1′, 3,3′tetraethylbenzimidazolylcarbocyanine iodide) and rhodamine-123 (Rh-123) dyes (Invitrogen). Cells were incubated with 1 μM of JC-1 dye or 10 μM of Rh-123 for 15 min at 37° C followed by washing of cells with PBS and examined under a fluorescence microscope (Olympus BX-60) to photograph with an attached Olympus digital camera (Optronics; Goleta, CA). ROS usually disrupts ΔΨm that can be measured with JC-1 dye with the shift of fluorescence from red to green. Green (Ex 485 nm, Em 535 nm) and red (Ex 540 nm, 590 nm) JC-1 signals indicate monomers and J-aggregates, respectively, in cells that were measured on a SpectroMax M5 microplate reader (Molecular Device, Sunnyvale, CA) and the ratio of J-aggregates to monomers was plotted. Likewise, cells incubated with Rh-123 were examined under a fluorescence microscope (Olympus BX-60) and photographed. Green (Ex 505 nm, Em 534 nm) Rh-123 signals of treated cells were measured on a SpectroMax M5 microplate reader (Molecular Device, Sunnyvale, CA) and results were plotted. Valinomycin (10 μM) was used as a positive control in all experiments (data not shown).

Measurement of ROCK and β-Galactosidase Activities

ROCK activity was measured in cell lysates by using a ROCK assay kit as instructed in the product manual (Millipore). Data are presented as absorbance in 200 μg of protein. Likewise, β-galactosidase reporter activity was measured in cell lysates by using a β-galactosidase reporter activity kit as per instructions in the product manual (Invitrogen, Carlsbad, CA).

Detection of Cell Death and Cell Viability

Cell death was determined by measuring lactate dehydrogenase (LDH) release in the culture supernatants using a LDH assay kit (Roche Diagnostics, Indianapolis, IN). Cell viability was measured by trypan blue exclusion using trypan blue (0.4%) in cells (1:1) and reading on TC10 automated cell counter (BIO-RAD).

Immunofluorescence

For single or double labeling, standard methodology was used. Briefly, slides were blocked by using an Image-iTV® fixation and permeabilization kit (Invitrogen) and incubated with appropriately diluted primary antibody (1:100) at 4° C overnight followed by washing and incubation with Alexa Fluor conjugated antibodies (1:500). Slides incubated with Alexa Fluor conjugated IgG antibodies without primary antibodies were negative control. Appropriate mouse IgG and rabbit polyclonal IgG antibodies were used as Isotype controls. After thorough washings, slides were mounted with Fluoromount-G (Electron Microscopy Sciences) containing Hoechst. Slides were analyzed by immunofluorescence microscopy (Olympus BX-60) with an Olympus digital camera (Optronics; Goleta, CA) using a dual-band pass filter. The contrast and brightness of images were processed using Adobe Photoshop CS 5 software.

Western Blotting

Cellular protein levels were measured by western blot analysis as previously described (Paintlia et al., 2005). Likewise, protein levels in cytosolic and nuclear fractions were measured as described earlier (Paintlia et al., 2008a). For co-immunoprecipitation, 200 μg of nuclear proteins were incubated with anti-CBP antibodies (20 μg) in 1 mL of PBS containing 0.01% Tween-20 for overnight at 4° C on orbital shaker. After 24 h, 50 μL (1.5 mg) of Dynabeads protein A (Enzo life Technologies, Grass Island, NY) were added and incubated for 10 min followed by collection of beads using magnet. Beads were washed twice with PBS/w Tween-20 and samples were analyzed by Western blot analysis. Autoradiographs were scanned and the band intensity was quantified by using image J software free download from the NIH (http://rsb.info.nih.gov/ij).

Transfection Studies

Lipofectamine was used for transfection of B12 cells in six-well cell culture plates. For PPRE reporter activity, cells were transiently transfected with 1–3 μg of each dominant-negative (DN) or constitutively active (CA) form of RhoA, cdc42, or Rac1 plasmids along with 0.3 μg of ptk-PPRE3-*luc* (kind gift from Dr. R. Evans, Salk Institute, La Jolla, CA) and 50 ng of pCMV-*βgal* (*β*-galactosidase; Clonetech, CA) plasmids. For chloramphenicol acetyltransferase (CAT) reporter activity, cells were transiently transfected with 1–3 μg of GAL4-UAS5-tk-CAT plasmids and the plasmid coding the nuclear receptor of interest (GAL4 DNA-BD/PPAR-α LBD, GAL4 DNA-BD/PPAR-β LBD, and GAL4 DNA-BD/PPAR-γ LBD) and 50 ng of pCMV-*βgal* plasmids as described previously (Kliewer et al., 1994). After 24 h, cells were cultured in fresh DMEM with 10% FBS for another 48 h followed by treatment with cytokines or pharmacological agents for the next 24 h and harvesting. Luciferase reporter activity was measured with a Luciferase assay kit (Promega, Madison, WI) and data were expressed relative to *β*-galactosidase activity. Likewise, CAT reporter activity in cell lysates was assessed by using a CAT enzyme assay system (Promega Corporation, Madison, WI) and the data were expressed as relative to *β*-galactosidase activity. For knockdown of PPAR subtypes gene expression in cells, 3.3 nmol of shRNA plasmids that generally consist of a pool of three to five lentiviral vector plasmids each encoding target-specific 19-25 nt (plus hairpin) shRNAs designed to knockdown the gene expression of PPAR-*α*/-*β*/-*γ* (Santa Cruz) were used. Control shRNA plasmids (Santa Cruz) that encodes a scrambled shRNA sequence that does not lead to the specific degradation of any cellular message were used. Knockdown of the targeted protein in cells was examined by Western blot analysis.

Quantitative Real-Time PCR Analysis

Cells were carefully processed for RNA isolation using TRIZOL reagent followed by cDNA synthesis and real-time PCR analysis using iCycler iQ Real-Time PCR Detection System (BIO-RAD Laboratories) as described previously (Paintlia et al., 2005). Gene-specific primers (Table 1) were designed using Primer Quest and purchased from Integrated DNA Technologies (Coralville, IA). Thermal cycling conditions were as follows: activation of iTaq™ DNA polymerase IQ™ in SYBR Green super mix at 95° C for 10 min, followed by 40 cycles of amplification at 95° C for 30 s and 59–60° C for 30 s. The specificity and detection methods for data analysis are as described earlier (Paintlia et al., 2008a).

Statistical Analysis

Data are given as the composite mean ± SE and analyzed using Student's *t* test or one-way multiple range analysis of variance (ANOVA) followed by a Bonferroni posttest for the comparison of all columns. *P* values were determined for three to four separate samples in

each experiment using GraphPad Prism 5.0 software (GraphPad Software, San Diego, CA). *P* values < 0.05 were considered significant.

Results

LOV Protects Vulnerable OLs from Cytokine Toxicity via PPARs Transactivation

Th1 and Th17 cytokines are known to play a significant role in EAE/MS pathogenesis (Brosnan and Raine, 1996; Gocke et al., 2007; Renno et al., 1995). Therefore, we here investigated the effect of the signatory cytokines of Th1 and Th17, i.e., TNF-α and IL-17, respectively, in OLs. We previously demonstrated that LOV protects OLs in mixed glial cultures stimulated with Th1 cytokines and in the EAE model (Paintlia et al., 2005, 2008a). In addition, we recently documented that IL-17 exacerbates TNF-α induced apoptotic cell death of OLs (Paintlia et al., 2011). Figure 1A depicts that LDH release was enhanced in the culture supernatants of OLs exposed to TNF-α and IL-17 compared with controls and that was attenuated by LOV treatment. This TNF-α plus IL-17-induced LDH release in the culture supernatants of OLs was greater than their individual treatment (Fig. 1A). Likewise, this cytokine-induced LDH release in the culture supernatants of B12 cells was attenuated by LOV (Supp. Info. Fig. 1A). This LOV-mediated protection of OLs from cytokine toxicity was measurable till eighth day posttreatment, however, that required changes of fresh media containing LOV plus cytokines every 72 h. Accordingly, MBP^{+ve} cell numbers were reduced in OL cultures exposed to cytokines that were rescued by LOV treatment (Fig. 1B). In addition, OLs differentiation was impaired due to cytokine toxicity as revealed by anti-MBP staining and that was reversed by LOV (Fig. 1C). Importantly, LOV plus cytokine treated OLs demonstrated thicker processes and more cytoplasm compared with controls (Fig. 1C). Likewise, LOV plus cytokine treated B12 cells demonstrated more processes compared with controls (Supp. Info. Fig. 1B). This LOV-mediated enhanced differentiation of OLs/B12 cells exposed to cytokines could be attributed to the controlled ROS generation, which are known to play an important role in the maturation of OLs (Cavaliere et al., 2012). These effects of LOV in OLs exposed to cytokine was reversed by L-mevalonate co-treatment (Fig. 1A,B), suggesting that the modulation of mevalonate pathway is crucial to protect OLs under pathological conditions.

We earlier documented that TNF-α- and IL-17-induced signaling mechanisms enhance ROS generation in OLs (Paintlia et al., 2011). Therefore, we next investigated whether LOV attenuates ROS generation in OLs exposed to cytokines. As expected, LOV attenuated ROS generation in OLs exposed to cytokines (Fig. 2A). It was true with similarly treated OLs with *N*-acetyl cysteine (NAC), a GSH precursor (Fig. 2A). Accordingly, the decreased GSH (reduced) level in OLs exposed to cytokines was reversed by NAC or LOV (Fig. 2B). In addition, cytokine-induced mitochondrial membrane depolarization in OLs was attenuated by LOV as revealed by the enhanced J-aggregates to monomers ratio (Fig. 2C) and the shift of JC-1 fluorescence emission from green to red (Fig. 2D). Likewise, LOV-mediated restoration of mitochondrial membrane potential in OLs exposed to cytokines was corroborated by another mitochondria specific Rh-123 dye staining (Supp. Info. Fig. 2A,B). Together, these data imply that LOV attenuates ROS generation thus protects mitochondria in OLs exposed to cytokines via restoration of GSH (reduced) level.

We next investigated the effect of LOV on the expression of ROS detoxifying enzymes, i.e., catalase (peroxisome) and SOD2 (mitochondrial), in similarly treated OLs. SOD2 is important to convert superoxide ($O_2\cdot$) into H_2O_2 and later is metabolized by catalase into H_2O (St-Pierre et al., 2006). Cytokine reduced levels of the catalase mRNA transcripts and protein in OLs compared with controls and that were reversed by LOV (Fig. 3A,C,D). Likewise, cytokine reduced the levels of *SOD2* mRNA transcripts and protein in OLs

compared with controls and that were reversed by LOV (Fig. 3B–D). These data suggest that LOV enhances ROS detoxifying defense in OLs to protect them from cytokine toxicity.

We next determined the transcriptional co-activation of transcription factors, i.e., PPARs and PGC-1α (co-activator), in similarly treated OLs which are known to participate in the expression of ROS detoxifying enzymes in cells (Baar, 2004; St-Pierre et al., 2006). The transcriptional co-activation of PPAR subtypes, i.e., PPAR-α/-β/-γ, as well as PGC-1α was increased in LOV-treated OLs in the presence or absence of cytokines than controls or OLs exposed to cytokines (Fig. 3E,F). Importantly, CBP interaction with PPAR-α and PGC-1α was greater than so with PPAR-β or PPAR-γ in LOV-treated OLs in the presence or absence of cytokines (Fig. 3E,F). These data suggest that LOV enhances ROS detoxifying defense in OLs via induction of PGC-1α and PPAR-α > PPAR-γ/or PPAR-β transactivation.

LOV Enhances PPARs Transactivation in OLs via Inhibition of Rho-ROCK Activity

Statins are reported to induce PPARs transactivation in different cell types (Landrier et al., 2004; Yano et al., 2007) and the statin-mediated induction of PPAR-γ transactivity via inhibition of RhoA activity participates in OLs differentiation (Miron et al., 2007; Paintlia et al., 2010). Therefore, it was of interest to investigate whether LOV-mediated inhibition of small Rho GTPases participates in the protection of OLs from cytokine toxicity. Statins inhibit small Rho GTPases activity in cells via inhibition of their membrane localization from cytoplasm due to impaired isoprenylation (Cordle et al., 2005). However, the GTP loading of small Rho GTPases, which is required for their activation, was not affected by statins in cells (Cordle et al., 2005). Therefore, we next measured the cytoplasmic levels of small Rho family GTPases, i.e., RhoA, cdc42, and Rac1, in treated OLs. Accumulation of RhoA and cdc42 proteins was enhanced in the cytoplasm of LOV-treated OLs in the presence or absence of cytokines than controls (Fig. 4A,B). However, Rac1 protein level in the cytoplasm was not affected in LOV-treated OLs, but it was enhanced in the presence of cytokines (Fig. 4A,B). ROCK activity was enhanced concomitantly in OLs exposed to cytokines compared with controls which were attenuated by LOV treatment (Fig. 4C). These data suggest that LOV inhibits Rho-ROCK activity in OLs exposed to cytokines.

Because the activities of small Rho GTPases and PPARs are inversely related in statin-treated OLs (Paintlia et al., 2010; Sim et al., 2008), we asked whether the observed PPARs transactivation in LOV-treated OLs is ascribed to the increased levels of their endogenous ligands. For this, we determined the activation of signaling mechanism that participates in the production of PPAR ligands in cells. The cPLA2 phosphorylation and COX-2 expression were enhanced in LOV-treated OLs in the presence or absence of cytokines compared with controls (Fig. 4D,E). These enzymes are reported to increase arachidonic acid release from phospholipids that eventually metabolized to produce endogenous PPAR ligands in cells (Pham et al., 2006; Xu et al., 2006). The phosphorylation of ERK (1/2) and p38 MAPK was also enhanced in similarly treated OLs (Fig. 4D,E). TNF-α and IL-17 are reported to induce p38 MAPK phosphorylation in cells (Li et al., 2007; Ma et al., 2010; Yagi et al., 2007). Therefore, cytokine induced p38 MAPK phosphorylation in OLs which was augmented by LOV treatment (Fig. 4D,E). These effects of LOV were mimicked by similarly treated OLs with ROCK inhibitor, Y27632 (Fig. 4D,E). Given the bioavailability of endogenous PPARs ligands is important to regulate the expression of their cognate transcription factors in cells (Bernardo et al., 2000), we next measured the expression of PPAR subtypes in treated OLs. Levels of PPAR-α and PPAR-γ, but not of PPAR-β mRNA, transcripts were reduced in OLs exposed to cytokines compared with controls which were reversed by LOV or Y27632 (Fig. 4F–H). Levels of all PPAR subtypes mRNA transcripts were however enhanced in control OLs treated with LOV or Y27632 (Fig. 4F–H). Consistent with primary OLs data, levels of PPAR subtypes mRNA transcripts were also altered in LOV-treated B12 cells in the

presence or absence of cytokines (Supp. Info. Fig. 1C). Altogether, these data suggest that the inhibition of Rho-ROCK activity enhances the level of PPARs ligands that, in turn, enhances their transactivation in LOV-treated OLs.

We next discerned which member of small Rho family GTPases is involved in PPARs transactivation in LOV-treated OLs (Fig. 3E,F). To address this, we modulated the activities of small Rho GTPases in B12 cells by transfecting them with plasmids that express constitutively active (CA) or dominant-negative (DN) forms of *Rho A*, *cdc42*, and *Rac1* along with plasmids that express luciferase (ptk-PPRE-*luc*) and *β*-galactosidase (pSV-*β*-*gal*) proteins. As reported earlier (Paintlia et al., 2010), PPRE reporter activity was enhanced in B12 cells transfected with control plasmids and treated with LOV or Y27632 in the presence or absence of cytokines (Fig. 5A). These effects of LOV in B12 cells exposed to cytokines were mimicked by transfection with *RhoA*-DN or *cdc42*-DN plasmids, but not with *Rac1*-DN plasmids (Fig. 5A). Importantly, LOV-induced PPRE reporter activity in B12 cells was reversed by transfection with RhoA-CA or cdc42-CA plasmids, but not with Rac1-CA plasmids (Fig. 5A). In addition, this LOV-induced PPRE reporter activity in B12 cells was attenuated by co-treatment with COX-2 inhibitor 1, arachidonyl trifluoromethyl ketone (cPLA2 inhibitor), and/or p38 MAPK inhibitor, SB203580 (Fig. 5A). Together, these data suggest that the inhibition of RhoA and cdc42 and thus ROCK activity is involved in PPARs transactivation in LOV-treated OLs via ERK (1/2)/p38 MAPK/cPLA2/COX-2 signaling cascade activation.

Comprehensive analysis using *PPAR-α/-β/-γ* GAL4/(UAS)5-CAT reporter system was performed to measure the endogenous levels of PPAR ligands in B12 cells. The GAL4-PPAR ligand binding domain (LBD) chimera reporter assay is very responsive to peroxisome proliferators (Wang et al., 2010). The CAT reporter activity was enhanced in LOV-treated B12 cells transfected with *PPAR-α*, *PPAR-β*, and/or *PPAR-γ* LBD plasmids compared with their respective controls (Fig. 5B). Importantly, the increased CAT reporter activity in LOV-treated B12 cells transfected with *PPAR-α* or *PPAR-γ* LBD plasmids was greater than those were transfected with *PPAR-β* LBD plasmids (Fig. 5B). This LOV-induced CAT reporter activity in B12 cells was mimicked by similar treatment with the agonists of PPAR-α (WY14643), PPAR-β (L165041), and/or PPAR-γ (ciglitazone) (Fig. 5B). In contrast, the LOV-induced CAT reporter activity in B12 cells was reversed by co-treatment with antagonists of PPAR-α (GW6471) or PPAR-γ GW9662) and/or SB203580 (Fig. 5C). PPAR-β antagonist was not available commercially at the time of study. These data show that the inhibition of Rho-ROCK activity increases the levels of PPAR ligands to a greater extent for PPAR-α and PPAR-γ than for PPAR-β in LOV-treated B12 cells via ERK (1/2)/p38 MAPK/cPLA2/COX-2 signaling activation.

LOV Enhances ROS Detoxifying Defense in OLs via PPAR-α-Dependent Mechanism

The above described findings demonstrate that LOV-mediated inhibition of Rho-ROCK activity enhances PPARs transactivation in OLs. It was of interest to discern which PPAR subtype is crucial to protect OLs from cytokine toxicity. To do this, we assessed the effect of LOV on ROS generation in B12 cells exposed to cytokines after depletion of PPAR-*α*/-*β*/or -*γ* proteins. As expected, cytokine-induced ROS generation in B12 cells transfected with control shRNA plasmids (scramble) was attenuated by LOV (Fig. 6A). This LOV-mediated attenuation of ROS generation was reversed in similarly treated B12 cells depleted of PPAR-α or PPAR-β, but not of PPAR-γ protein (Fig. 6A). Importantly, cytokine-induced ROS generation was enhanced in B12 cells depleted of PPAR-α or PPAR-β protein compared with controls or those were depleted of PPAR-γ protein (Fig. 6A). This observed LOV-mediated attenuation of ROS generation in B12 cells was reverted by transfection with *RhoA*-CA plasmids (Fig. 6A). Like treatment with LOV, the observed cytokine-induced

ROS generation in B12 cells was attenuated by transfection with *RhoA*-DN plasmids (Fig. 6A). Together, these data indicate that Rho-ROCK activity inhibition attenuates oxidative stress in LOV-treated B12 cells via PPAR-α or PPAR-β transactivation.

We next asked whether PPAR-α or PPAR-β is involved in the expression of ROS detoxifying enzymes in LOV-treated OLs. To address this question, the expression of *catalase* and *SOD2* genes was determined in LOV-treated B12 cells depleted of PPAR subtypes using shRNA plasmids based transfections. There were increased levels of both *catalase* and *SOD2* mRNA transcripts in LOV-treated B12 cells compared with controls which were reverted by depletion of PPAR-α protein (Fig. 6B). In contrast, LOV-mediated increased *catalase* and *SOD2* expression was unaffected in B12 cells depleted of PPAR-β or PPAR-γ protein (Fig. 6B). However, level of *catalase* mRNA transcripts was increased $\simeq$2-fold in LOV-treated B12 cells depleted of PPAR-γ protein compared with controls (Fig. 6B). Levels of *catalase* and *SOD2* mRNA transcripts were also elevated in B12 cells depleted of each PPAR subtype compared with controls (Fig. 6B). Together, these data provide evidence that PPAR-α transactivation is crucial to enhance ROS detoxifying defense in LOV-treated OLs.

To determine whether gene redundancy is responsible for the regulation of ROS detoxifying defense in LOV-treated B12 cells, PPRE reporter activity was measured in LOV-treated B12 cells depleted of each PPAR subtype using shRNA plasmids based transfections. LOV-induced PPRE reporter activity in B12 cells transfected with control shRNA plasmids was reduced remarkably by depletion of PPAR-α or PPAR-β protein (Fig. 7A). This LOV-induced PPRE reporter activity was also reduced significantly ($P < 0.05$) in B12 cells depleted of PPAR-γ protein, but it was not as impressive as observed in B12 cells depleted of PPAR-α or PPAR-β protein (Fig. 7A). These PPRE reporter activity data were consistent with the reduced level of each PPAR subtype mRNA transcripts in LOV-treated B12 cells depleted of each PPAR subtype protein (Fig. 7B). Importantly, LOV increased the levels of each PPAR subtypes mRNA transcripts in B12 cells transfected with control shRNA plasmids which were reversed by depletion of respective PPAR subtype protein (Fig. 7B). Consistent with mRNA data, Western blotting demonstrated the reduced level of each PPAR subtype in LOV-treated B12 cells transfected with respective shRNA plasmids (Fig. 7C). Interestingly, levels of *PPAR-*α and/or both *PPAR-*α and *PPAR-*β mRNA transcripts and protein were especially enhanced in LOV-treated B12 cells depleted of PPAR-β or PPAR-γ proteins, respectively (Fig. 7B,C). Double knockdown of PPAR subtypes, i.e., PPAR-α plus PPAR-γ or PPAR-γ plus PPAR-β and/or PPAR-α plus PPAR-β, proteins in B12 cells further demonstrated that the reduced LOV-induced PPRE reporter activity in B12 cells depleted of single PPAR subtype protein was worsened by depletion of two PPAR subtype proteins (Fig. 7D). Western blotting demonstrated the reduced levels of PPAR subtype proteins in LOV-treated B12 cells depleted of two PPAR subtypes proteins (Fig. 7C). These data provide evidence that the observed alterations in LOV-induced PPRE reporter activity in B12 cells depleted of single PPAR subtype protein is attributed to gene redundancy (Fig. 7D) and suggesting that LOV greatly influences PPAR-α than so PPAR-β or PPAR-γ transactivation in OLs/B12 cells.

To further confirm these findings that PPAR-α transactivation participates in OL protection from cytokine toxicity, we assessed the effect of LOV in WT and *PPAR-*α deficient OLs exposed to cytokines. As expected, the observed LOV-mediated protection of OLs (WT) from cytokine toxicity was lacking in similarly treated *PPAR-*α deficient OLs as revealed by LDH release (Fig. 8A) and by trypan blue exclusion assays (data not shown). Importantly, cytokine toxicity was severe in PPAR-α deficient OLs compared with WT OLs (Fig. 8A). Consistent with OL survival data, LOV-mediated increase in the number of MBP^{+ve} cells in WT OLs exposed to cytokines was reversed in similarly treated *PPAR-*α deficient OLs (Fig.

8B). Together, these data reinforce our conclusions that LOV protects OLs from cytokine toxicity via PPAR-α transactivation.

Discussion

The present study extends our previous observations (Paintlia et al., 2005, 2008a) and demonstrates that LOV-mediated inhibition of Rho-ROCK activity enhances ROS detoxifying defense in OLs to protect them from cytokine toxicity. Our findings demonstrate for the first time that the inhibition of small Rho GTPases, i.e., RhoA and cdc42, thus ROCK activity enhances PPARs transactivation in OLs (Figs. 3E,F, 4, and 5). Characteristically, small Rho GTPases are reported to regulate actin-binding proteins that are involved in the regulation of the dynamics of the actin cytoskeleton in cells (Cordle et al., 2005). RhoA controls the formation of contractile stress fibers and focal adhesions (Liang et al., 2004; Osterhout et al., 1999). Rac1 participates in membrane ruffling, cell motility, and actin polymerization, while cdc42 participates in filopodia formation and cell–cell adhesions (Liang et al., 2004). Rac1 as the subunit of NADPH oxidase participates in the generation of ROS in cells, which are reported to be inhibited by statins (Maack et al., 2003). In agreement with this, we observed the inhibition of cytokine-induced Rac1 activity in LOV-treated OLs exposed to cytokines (Fig. 4A,B). It was accompanied with LOV-mediated attenuation of ROS generation and the mitochondrial membrane depolarization in OLs (Fig. 2A–D; Supp. Info. Fig. 2A,B). In addition, LOV or NAC treatment reversed the cytokine mediated lowering of GSH (reduced) level in OLs (Fig. 2B). The expression of catalase (peroxisome) and SOD2 (mitochondria) (Fig. 3A–D) and the transactivation of PGC-1α and PPARs (Fig. 3E,F) were enhanced in LOV-treated OLs. PGC-1α is reported to suppress ROS generation and limit neurodegeneration under pathological conditions (Baar, 2004; St-Pierre et al., 2006). Statin-mediated inhibition of RhoA is reported to enhance PPAR-γ transactivation in cells under pathological conditions (Shen et al., 2010; Yano et al., 2007). We found that LOV-mediated induction of PPAR transactivation in OLs is ascribed to the inhibition of RhoA and cdc42 and thus ROCK activity (Figs. 4 and 5). By combining biochemical and genetic approaches, we demonstrated that LOV-mediated induction of PPAR-α transactivation boosts ROS detoxifying defense in OLs (Fig. 6A,B). However, further studies are required to determine a possible link that may exist between activities of small Rho GTPases and PPAR-α in *in vivo* using OL specific conditional knockout mice for RhoA or cdc42 protein.

PPARs are known to regulate the gene activity of key enzymes involved in the lipid metabolism of cells (Amri et al., 1995; Forman et al., 1995). In addition, PPARs are reported to exhibit anti-inflammatory activities in glial cells and their protective effects in various neurodegenerative disorders (Defaux et al., 2009; Paintlia et al., 2006). PPAR transactivation in cells is largely regulated by the bioavailability of their natural ligands, produced by COX-2 via p38 MAPK-dependent mechanism (Pham et al., 2006; Yano et al., 2007). The cPLA2 is reported to increase the release of arachidonic acid from phospholipids, the substrate for COX-2 to produce endogenous PPAR ligands in cells (Smith et al., 2002, 2005). In agreement with this, we observed the increased expression of COX-2 and the enhanced phosphorylation of cPLA2 in LOV-treated OLs (Fig. 4D,E). It was accompanied with the increased phosphorylation of ERK (1/2) and p38 MAPK in similarly treated OLs (Fig. 4D,E). The activation (phosphorylation) of p38 MAPK and ERK (1/2) is reported to increase the phosphorylation of cPLA2 (Borsch-Haubold et al., 1998; Siegel et al., 2001). In agreement with this, we found that LOV increases the bioavailability of endogenous PPAR ligands in B12 cells as revealed by the CAT reporter activity assay (Fig. 5B,C) and the induction of PPARs expression in LOV-treated OLs or B12 cells (Fig. 4F–H; Supp. Info. Fig. 1C). We concluded that LOV enhances the production of PPAR ligands in OLs via activation of ERK (1/2)-p38 MAPK-cPLA2-COX-2 signaling cascade.

Interestingly, LOV-mediated attenuation of ROS generation in B12 cells exposed to cytokines was reversed by the depletion of PPAR-α or PPAR-β protein (Fig. 6A). In contrast, this effect of LOV on ROS generation in B12 cells exposed to cytokines was unaffected by the depletion of PPAR-γ protein (Fig. 6A). The exact cause of the observed variation in ROS generation in LOV-treated B12 cells exposed to cytokines after depletion of PPAR-γ protein may be due to gene redundancy (Fig. 7A–D). Our conclusions are supported by the increased expression of catalase and SOD2 in LOV-treated B12 cells after depletion of PPAR-γ protein (Fig. 6B). It suggests a positive feedback loop that may exist in cells and that allows the endogenous activators to sustain the responsiveness of these cells by increasing the expression of their cognate receptors. Secondly, the observed enhanced PPAR-α expressions with a corresponding increase in the expression of catalase and SOD2 in LOV-treated B12 cells depleted of PPAR-γ or PPAR-β proteins (Fig. 6B) is suggesting that LOV-mediated induction of PPAR-α transactivation is crucial to protect OLs from cytokine toxicity. These conclusions were further reinforced by the absence of LOV-mediated protective effects in OLs deficient of PPAR-α from cytokine toxicity (Fig. 8A,B). In support of this, we earlier documented that NAC treatment protects OLs against cytokine toxicity via PPAR-α-dependent mechanism (Paintlia et al., 2008c). In addition, PPAR-α transactivation is reported to mediate the anti-inflammatory activities of statin in different disease models (Esposito et al., 2012; Rinaldi et al., 2011).

Importantly, PPARs are known to regulate ROS detoxifying defense and the expression of proteins for cellular organelles, i.e., peroxisomes and mitochondria (Liao et al., 2008; Williams et al., 2008). The observed LOV-mediated increase in the expression of catalase and SOD2 accompanied with the induction of PGC-1α and PPAR-β co-transactivation (Fig. 3E,F) are suggestive of an increase in the density of peroxisomes/mitochondria in OLs. In support of this, we earlier documented that LOV attenuates impaired peroxisomal functions in the EAE model (Singh et al., 2004). NAC treatment attenuated the peroxisomal dysfunctions in the white matter injury model via PPAR-α-dependent mechanism (Paintlia et al., b,c). The biogenesis of organelles, i.e., peroxisomes and mitochondria, and the suppression of ROS generation in cells are reported to be regulated by PPARs and PGC-1α transactivation (Baar, 2004; St-Pierre et al., 2006). P38 MAPK is an important inducer of PGC-1α transactivation in cells (Akimoto et al., 2005). We found that the phosphorylation of ERK (1/2) and p38 MAPK (Fig. 4D,E) and the PGC-1α transactivation (Fig. 3E,F) were concomitantly enhanced in OLs by LOV. Recent studies provide evidence that the functioning of mitochondria and peroxisomes exhibits a closer relationship. For instance, the inhibition of peroxisomal catalase activity not only enhances H_2O_2 levels thus peroxisomal dysfunction, but that consequently inhibits mitochondrial functions as evidenced by an increase in the level of mitochondrial ROS generation and the mitochondrial membrane depolarization in cells (Koepke et al., 2008). In line with this, the inhibition of catalase activity in human fibroblasts showed mitochondrial aconitase activity inhibition by 85% with a concomitant increase in mitochondrial ROS production (Walton and Pizzitelli, 2012). Moreover, the absence of functional peroxisomes in the CNS is reported to cause demyelination and axonal damage as well as the ablation of PGC-1α is reported to increase the susceptibility of neuron to oxidative injury (Camacho et al., 2012; Hulshagen et al., 2008). In light of these data and our findings, we surmise that LOV-mediated induction of PPAR-α and PGC-1α transactivation may enhance the density of peroxisome and mitochondria to enhance ROS detoxifying defense in OLs. However, detailed investigations in this context are warranted.

In summary, the present study describes the novel role of Rho-ROCK activity in the regulation of ROS detoxifying defense in OLs. LOV-mediated inhibition of Rho-ROCK activity induces PPAR-α- and PGC-1α-dependent transcriptional activities to enhance catalase (peroxisome) and SOD2 (mitochondria) expression in OLs to protect them from

cytokine toxicity (Fig. 9). These findings open up new avenues in the investigation of PPAR-α agonists especially those can cross the blood–brain barrier as standalone therapy or in combination with statins or ROCK inhibitors (fasudil) in MS and related neurodegenerative disorders.

Supplementary Material

Refer to Web version on PubMed Central for supplementary material.

Acknowledgments

Grant sponsor: National Institutes of Health; Grant numbers: NS-22576, NS-37766, and C06 RR018823; Grant sponsor: Department of Veterans Affairs; Grant numbers: VA-1BX001072 and VA-BX001999.

We thank especially Ms. Joyce Brian for her technical assistance.

Abbreviations

CAT	chloramphenicol acetyl transferase
EAE	experimental autoimmune encephalomyelitis
LDH	lactate dehydrogenase
LOV	lovastatin
PDL	poly-D-lysine
PGC-1α	PPAR-γ co-activator 1α
PPAR	peroxisome proliferators activated receptor
ROCK	Rho-associated kinase
ROS	reactive oxygen species
SOD2	superoxide dismutase

References

Akimoto T, Pohnert SC, Li P, Zhang M, Gumbs C, Rosenberg PB, Williams RS, Yan Z. Exercise stimulates Pgc-1alpha transcription in skeletal muscle through activation of the p38 MAPK pathway. J Biol Chem. 2005; 280:19587–19593. [PubMed: 15767263]

Amri EZ, Bonino F, Ailhaud G, Abumrad NA, Grimaldi PA. Cloning of a protein that mediates transcriptional effects of fatty acids in preadipocytes. Homology to peroxisome proliferator-activated receptors. J Biol Chem. 1995; 270:2367–2371. [PubMed: 7836471]

Andrews T, Zhang P, Bhat NR. TNFalpha potentiates IFNgamma-induced cell death in oligodendrocyte progenitors. J Neurosci Res. 1998; 54:574– 583. [PubMed: 9843148]

Baar K. Involvement of PPAR gamma co-activator-1, nuclear respiratory factors 1 and 2, and PPAR alpha in the adaptive response to endurance exercise. Proc Nutr Soc. 2004; 63:269–273. [PubMed: 15294042]

Bernardo A, Levi G, Minghetti L. Role of the peroxisome proliferator-activated receptor-gamma (PPAR-gamma) and its natural ligand 15-deoxy-Delta12, 14-prostaglandin J2 in the regulation of microglial functions. Eur J Neurosci. 2000; 12:2215–2223. [PubMed: 10947800]

Borsch-Haubold AG, Bartoli F, Asselin J, Dudler T, Kramer RM, Apitz-Castro R, Watson SP, Gelb MH. Identification of the phosphorylation sites of cytosolic phospholipase A2 in agonist-stimulated human platelets and HeLa cells. J Biol Chem. 1998; 273:4449–4458. [PubMed: 9468497]

Bottenstein JE, Sato GH. Growth of a rat neuroblastoma cell line in serum-free supplemented medium. Proc Natl Acad Sci USA. 1979; 76:514–517. [PubMed: 284369]

Brosnan CF, Raine CS. Mechanisms of immune injury in multiple sclerosis. Brain Pathol. 1996; 6:243–257. [PubMed: 8864282]

Calderon FH, von Bernhardi R, De Ferrari G, Luza S, Aldunate R, Inestrosa NC. Toxic effects of acetylcholinesterase on neuronal and glial-like cells in vitro. Mol Psychiatry. 1998; 3:247–255. [PubMed: 9672900]

Camacho A, Rodriguez-Cuenca S, Blount M, Prieur X, Barbarroja N, Fuller M, Hardingham GE, Vidal-Puig A. Ablation of PGC1 beta prevents mTOR dependent endoplasmic reticulum stress response. Exp Neurol. 2012; 237:396–406. [PubMed: 22771762]

Cavaliere F, Urra O, Alberdi E, Matute C. Oligodendrocyte differentiation from adult multipotent stem cells is modulated by glutamate. Cell Death Dis. 2012; 3:e268. [PubMed: 22297298]

Cordle A, Koenigsknecht-Talboo J, Wilkinson B, Limpert A, Landreth G. Mechanisms of statin-mediated inhibition of small G-protein function. J Biol Chem. 2005; 280:34202–34209. [PubMed: 16085653]

Defaux A, Zurich MG, Braissant O, Honegger P, Monnet-Tschudi F. Effects of the PPAR-beta agonist GW501516 in an in vitro model of brain inflammation and antibody-induced demyelination. J Neuroinflammation. 2009; 6:15. [PubMed: 19422681]

Dunn SE, Bhat R, Straus DS, Sobel RA, Axtell R, Johnson A, Nguyen K, Mukundan L, Moshkova M, Dugas JC, Chawla A, Steinman L. Peroxisome proliferator-activated receptor delta limits the expansion of pathogenic Th cells during central nervous system autoimmunity. J Exp Med. 2010; 207:1599–1608. [PubMed: 20624891]

Dunn SE, Youssef S, Goldstein MJ, Prod'homme T, Weber MS, Zamvil SS, Steinman L. Isoprenoids determine Th1/Th2 fate in pathogenic T cells, providing a mechanism of modulation of autoimmunity by atorvastatin. J Exp Med. 2006; 203:401–412. [PubMed: 16476765]

Esposito E, Rinaldi B, Mazzon E, Donniacuo M, Impellizzeri D, Paterniti I, Capuano A, Bramanti P, Cuzzocrea S. Anti-inflammatory effect of simvastatin in an experimental model of spinal cord trauma: Involvement of PPAR-alpha. J Neuroinflammation. 2012; 9:81. [PubMed: 22537532]

Floris S, Blezer EL, Schreibelt G, Dopp E, van der Pol SM, Schadee-Eester-mans IL, Nicolay K, Dijkstra CD, de Vries HE. Blood-brain barrier permeability and monocyte infiltration in experimental allergic encephalomyelitis: A quantitative MRI study. Brain. 2004; 127:616–627. [PubMed: 14691063]

Forman BM, Tontonoz P, Chen J, Brun RP, Spiegelman BM, Evans RM. 15-Deoxy-delta 12, 14-prostaglandin J2 is a ligand for the adipocyte determination factor PPAR gamma. Cell. 1995; 83:803–812. [PubMed: 8521497]

Funfschilling U, Supplie LM, Mahad D, Boretius S, Saab AS, Edgar J, Brink-mann BG, Kassmann CM, Tzvetanova ID, Mobius W, et al. Glycolytic oligodendrocytes maintain myelin and long-term axonal integrity. Nature. 2012; 485:517–521. [PubMed: 22622581]

Gocke AR, Cravens PD, Ben LH, Hussain RZ, Northrop SC, Racke MK, Lovett-Racke AE. T-bet regulates the fate of Th1 and Th17 lymphocytes in autoimmunity. J Immunol. 2007; 178:1341–1348. [PubMed: 17237380]

Greenwood J, Walters CE, Pryce G, Kanuga N, Beraud E, Baker D, Adamson P. Lovastatin inhibits brain endothelial cell Rho-mediated lymphocyte migration and attenuates experimental autoimmune encephalomyelitis. FASEB J. 2003; 17:905–907. [PubMed: 12626426]

Hulshagen L, Krysko O, Bottelbergs A, Huyghe S, Klein R, Van Veldhoven PP, De Deyn PP, D'Hooge R, Hartmann D, Baes M. Absence of functional peroxisomes from mouse CNS causes dysmyelination and axon degeneration. J Neurosci. 2008; 28:4015–4027. [PubMed: 18400901]

Keelan J, Allen NJ, Antcliffe D, Pal S, Duchen MR. Quantitative imaging of glutathione in hippocampal neurons and glia in culture using monochlorobimane. J Neurosci Res. 2001; 66:873–884. [PubMed: 11746414]

Kliewer SA, Forman BM, Blumberg B, Ong ES, Borgmeyer U, Mangelsdorf DJ, Umesono K, Evans RM. Differential expression and activation of a family of murine peroxisome proliferator-activated receptors. Proc Natl Acad Sci USA. 1994; 91:7355–7359. [PubMed: 8041794]

Klotz L, Burgdorf S, Dani I, Saijo K, Flossdorf J, Hucke S, Alferink J, Nowak N, Beyer M, Mayer G, Langhans B, Klockgether T, Waisman A, Eberl G, Schultze J, Famulok M, Kolanus W, Glass C, Kurts C, Knolle PA. The nuclear receptor PPAR gamma selectively inhibits Th17 differentiation

in a T cell-intrinsic fashion and suppresses CNS autoimmunity. J Exp Med. 2009; 206:2079–2089. [PubMed: 19737866]

Koepke JI, Wood CS, Terlecky LJ, Walton PA, Terlecky SR. Progeric effects of catalase inactivation in human cells. Toxicol Appl Pharmacol. 2008; 232:99–108. [PubMed: 18634817]

Landrier JF, Thomas C, Grober J, Duez H, Percevault F, Souidi M, Linard C, Staels B, Besnard P. Statin induction of liver fatty acid-binding protein (L-FABP) gene expression is peroxisome proliferator-activated receptor-alpha-dependent. J Biol Chem. 2004; 279:45512–45518. [PubMed: 15337740]

Li G, Barrett EJ, Barrett MO, Cao W, Liu Z. Tumor necrosis factor-alpha induces insulin resistance in endothelial cells via a p38 mitogen-activated protein kinase-dependent pathway. Endocrinology. 2007; 148:3356–3363. [PubMed: 17446186]

Liang X, Draghi NA, Resh MD. Signaling from integrins to Fyn to Rho family GTPases regulates morphologic differentiation of oligodendrocytes. J Neurosci. 2004; 24:7140–7149. [PubMed: 15306647]

Liao BC, Hsieh CW, Liu YC, Tzeng TT, Sun YW, Wung BS. Cinnamaldehyde inhibits the tumor necrosis factor-alpha-induced expression of cell adhesion molecules in endothelial cells by suppressing NF-kappaB activation: Effects upon IkappaB and Nrf2. Toxicol Appl Pharmacol. 2008; 229:161–171. [PubMed: 18304597]

Ma X, Reynolds SL, Baker BJ, Li X, Benveniste EN, Qin H. IL-17 enhancement of the IL-6 signaling cascade in astrocytes. J Immunol. 2010; 184:4898–4906. [PubMed: 20351184]

Maack C, Kartes T, Kilter H, Schafers HJ, Nickenig G, Bohm M, Laufs U. Oxygen free radical release in human failing myocardium is associated with increased activity of rac1-GTPase and represents a target for statin treatment. Circulation. 2003; 108:1567–1574. [PubMed: 12963641]

Miron VE, Rajasekharan S, Jarjour AA, Zamvil SS, Kennedy TE, Antel JP. Simvastatin regulates oligodendroglial process dynamics and survival. Glia. 2007; 55:130–143. [PubMed: 17078030]

Oluich LJ, Stratton JA, Lulu Xing Y, Ng SW, Cate HS, Sah P, Windels F, Kilpa-trick TJ, Merson TD. Targeted ablation of oligodendrocytes induces axonal pathology independent of overt demyelination. J Neurosci. 2012; 32:8317–8330. [PubMed: 22699912]

Osterhout DJ, Wolven A, Wolf RM, Resh MD, Chao MV. Morphological differentiation of oligodendrocytes requires activation of Fyn tyrosine kinase. J Cell Biol. 1999; 145:1209–1218. [PubMed: 10366594]

Paintlia AS, Paintlia MK, Khan M, Vollmer T, Singh AK, Singh I. HMGCoA reductase inhibitor augments survival and differentiation of oligodendrocyte progenitors in animal model of multiple sclerosis. FASEB J. 2005; 19:1407–1421. [PubMed: 16126908]

Paintlia AS, Paintlia MK, Singh AK, Orak JK, Singh I. Activation of PPAR-gamma and PTEN cascade participates in lovastatin-mediated accelerated differentiation of oligodendrocyte progenitor cells. Glia. 2010; 58:1669–1685. [PubMed: 20578043]

Paintlia AS, Paintlia MK, Singh AK, Singh I. Inhibition of rho family functions by lovastatin promotes myelin repair in ameliorating experimental autoimmune encephalomyelitis. Mol Pharmacol. 2008a; 73:1381–1393. [PubMed: 18239032]

Paintlia AS, Paintlia MK, Singh I, Singh AK. IL-4-induced peroxisome proliferator-activated receptor gamma activation inhibits NF-kappaB trans activation in central nervous system (CNS) glial cells and protects oligodendrocyte progenitors under neuroinflammatory disease conditions: Implication for CNS-demyelinating diseases. J Immunol. 2006; 176:4385–4398. [PubMed: 16547277]

Paintlia MK, Paintlia AS, Contreras MA, Singh I, Singh AK. Lipopolysaccharide-induced peroxisomal dysfunction exacerbates cerebral white matter injury: Attenuation by N-acetyl cysteine. Exp Neurol. 2008b; 210:560–576. [PubMed: 18291369]

Paintlia MK, Paintlia AS, Khan M, Singh I, Singh AK. Modulation of peroxisome proliferator-activated receptor-alpha activity by N-acetyl cysteine attenuates inhibition of oligodendrocyte development in lipopolysaccharide stimulated mixed glial cultures. J Neurochem. 2008c; 105:956–970. [PubMed: 18205750]

Paintlia MK, Paintlia AS, Singh AK, Singh I. Synergistic activity of interleukin-17 and tumor necrosis factor-alpha enhances oxidative stress-mediated oligodendrocyte apoptosis. J Neurochem. 2011; 116:508–521. [PubMed: 21143599]

Paintlia MK, Paintlia AS, Singh AK, Singh I. S-nitrosoglutathione induces ciliary neurotrophic factor expression in astrocytes, which has implications to protect the central nervous system under pathological conditions. J Biol Chem. 2013; 288:3831–3843. [PubMed: 23264628]

Pang Y, Cai Z, Rhodes PG. Effect of tumor necrosis factor-alpha on developing optic nerve oligodendrocytes in culture. J Neurosci Res. 2005; 80:226–234. [PubMed: 15765524]

Pham H, Shafer LM, Slice LW. CREB-dependent cyclooxygenase-2 and microsomal prostaglandin E synthase-1 expression is mediated by protein kinase C and calcium. J Cell Biochem. 2006; 98:1653–1666. [PubMed: 16598755]

Renno T, Krakowski M, Piccirillo C, Lin JY, Owens T. TNF-alpha expression by resident microglia and infiltrating leukocytes in the central nervous system of mice with experimental allergic encephalomyelitis. Regulation by Th1 cytokines. J Immunol. 1995; 154:944–953. [PubMed: 7814894]

Rinaldi B, Donniacuo M, Esposito E, Capuano A, Sodano L, Mazzon E, Di Palma D, Paterniti I, Cuzzocrea S, Rossi F. PPARalpha mediates the anti-inflammatory effect of simvastatin in an experimental model of zymosan-induced multiple organ failure. Br J Pharmacol. 2011; 163:609–623. [PubMed: 21323892]

Roth AD, Leisewitz AV, Jung JE, Cassina P, Barbeito L, Inestrosa NC, Bronfman M. PPAR gamma activators induce growth arrest and process extension in B12 oligodendrocyte-like cells and terminal differentiation of cultured oligodendrocytes. J Neurosci Res. 2003; 72:425–435. [PubMed: 12704804]

Saluja I, Granneman JG, Skoff RP. PPAR delta agonists stimulate oligodendrocyte differentiation in tissue culture. Glia. 2001; 33:191–204. [PubMed: 11241737]

Shen Y, Wu H, Wang C, Shao H, Huang H, Jing H, Li D. Simvastatin attenuates cardiopulmonary bypass-induced myocardial inflammatory injury in rats by activating peroxisome proliferator-activated receptor gamma. Eur J Pharmacol. 2010; 649:255–262. [PubMed: 20858481]

Siegel G, Sternfeld L, Gonzalez A, Schulz I, Schmid A. Arachidonic acid modulates the spatiotemporal characteristics of agonist-evoked Ca21 waves in mouse pancreatic acinar cells. J Biol Chem. 2001; 276:16986–16991. [PubMed: 11279177]

Sim FJ, Lang JK, Ali TA, Roy NS, Vates GE, Pilcher WH, Goldman SA. Statin treatment of adult human glial progenitors induces PPAR gamma-mediated oligodendrocytic differentiation. Glia. 2008; 56:954–962. [PubMed: 18383345]

Singh I, Pahan K, Khan M, Singh AK. Cytokine-mediated induction of ceramide production is redox-sensitive. Implications to proinflammatory cytokine-mediated apoptosis in demyelinating diseases. J Biol Chem. 1998; 273:20354–20362. [PubMed: 9685387]

Singh I, Paintlia AS, Khan M, Stanislaus R, Paintlia MK, Haq E, Singh AK, Contreras MA. Impaired peroxisomal function in the central nervous system with inflammatory disease of experimental autoimmune encephalomyelitis animals and protection by lovastatin treatment. Brain Res. 2004; 1022:1–11. [PubMed: 15353207]

Smith LH, Boutaud O, Breyer M, Morrow JD, Oates JA, Vaughan DE. Cyclooxygenase-2-dependent prostacyclin formation is regulated by low density lipoprotein cholesterol in vitro. Arterioscler Thromb Vasc Biol. 2002; 22:983–988. [PubMed: 12067908]

Smith LH, Petrie MS, Morrow JD, Oates JA, Vaughan DE. The sterol response element binding protein regulates cyclooxygenase-2 gene expression in endothelial cells. J Lipid Res. 2005; 46:862–871. [PubMed: 15716578]

Soulika AM, Lee E, McCauley E, Miers L, Bannerman P, Pleasure D. Initiation and progression of axonopathy in experimental autoimmune encephalomyelitis. J Neurosci. 2009; 29:14965–14979. [PubMed: 19940192]

St-Pierre J, Drori S, Uldry M, Silvaggi JM, Rhee J, Jager S, Handschin C, Zheng K, Lin J, Yang W, et al. Suppression of reactive oxygen species and neurodegeneration by the PGC-1 transcriptional coactivators. Cell. 2006; 127:397–408. [PubMed: 17055439]

Vollmer T, Key L, Durkalski V, Tyor W, Corboy J, Markovic-Plese S, Preiningerova J, Rizzo M, Singh I. Oral simvastatin treatment in relapsing-remitting multiple sclerosis. Lancet. 2004; 363:1607–1608. [PubMed: 15145635]

Walton PA, Pizzitelli M. Effects of peroxisomal catalase inhibition on mitochondrial function. Front Physiol. 2012; 3:108. [PubMed: 22536190]

Wang S, Zhang M, Liang B, Xu J, Xie Z, Liu C, Viollet B, Yan D, Zou MH. AMPKalpha2 deletion causes aberrant expression and activation of NAD(P)H oxidase and consequent endothelial dysfunction in vivo: Role of 26S proteasomes. Circ Res. 2010; 106:1117–1128. [PubMed: 20167927]

Williams MA, Rangasamy T, Bauer SM, Killedar S, Karp M, Kensler TW, Yamamoto M, Breysse P, Biswal S, Georas SN. Disruption of the transcription factor Nrf2 promotes pro-oxidative dendritic cells that stimulate Th2-like immunoresponsiveness upon activation by ambient particulate matter. J Immunol. 2008; 181:4545–4559. [PubMed: 18802057]

Woods JW, Tanen M, Figueroa DJ, Biswas C, Zycband E, Moller DE, Austin CP, Berger JP. Localization of PPARdelta in murine central nervous system: Expression in oligodendrocytes and neurons. Brain Res. 2003; 975:10–21. [PubMed: 12763589]

Xu L, Han C, Lim K, Wu T. Cross-talk between peroxisome proliferator-activated receptor delta and cytosolic phospholipase A(2)alpha/cyclooxygenase-2/prostaglandin E(2) signaling pathways in human hepatocellular carcinoma cells. Cancer Res. 2006; 66:11859–11868. [PubMed: 17178883]

Yagi Y, Andoh A, Inatomi O, Tsujikawa T, Fujiyama Y. Inflammatory responses induced by interleukin-17 family members in human colonic subepithelial myofibroblasts. J Gastroenterol. 2007; 42:746–753. [PubMed: 17876544]

Yano M, Matsumura T, Senokuchi T, Ishii N, Murata Y, Taketa K, Motoshima H, Taguchi T, Sonoda K, Kukidome D, et al. Statins activate peroxisome proliferator-activated receptor gamma through extracellular signal-regulated kinase 1/2 and p38 mitogen-activated protein kinase-dependent cyclooxygenase-2 expression in macrophages. Circ Res. 2007; 100:1442–1451. [PubMed: 17463321]

Youssef S, Stuve O, Patarroyo JC, Ruiz PJ, Radosevich JL, Hur EM, Bravo M, Mitchell DJ, Sobel RA, Steinman L, et al. The HMG-CoA reductase inhibitor, atorvastatin, promotes a Th2 bias and reverses paralysis in central nervous system autoimmune disease. Nature. 2002; 420:78–84. [PubMed: 12422218]

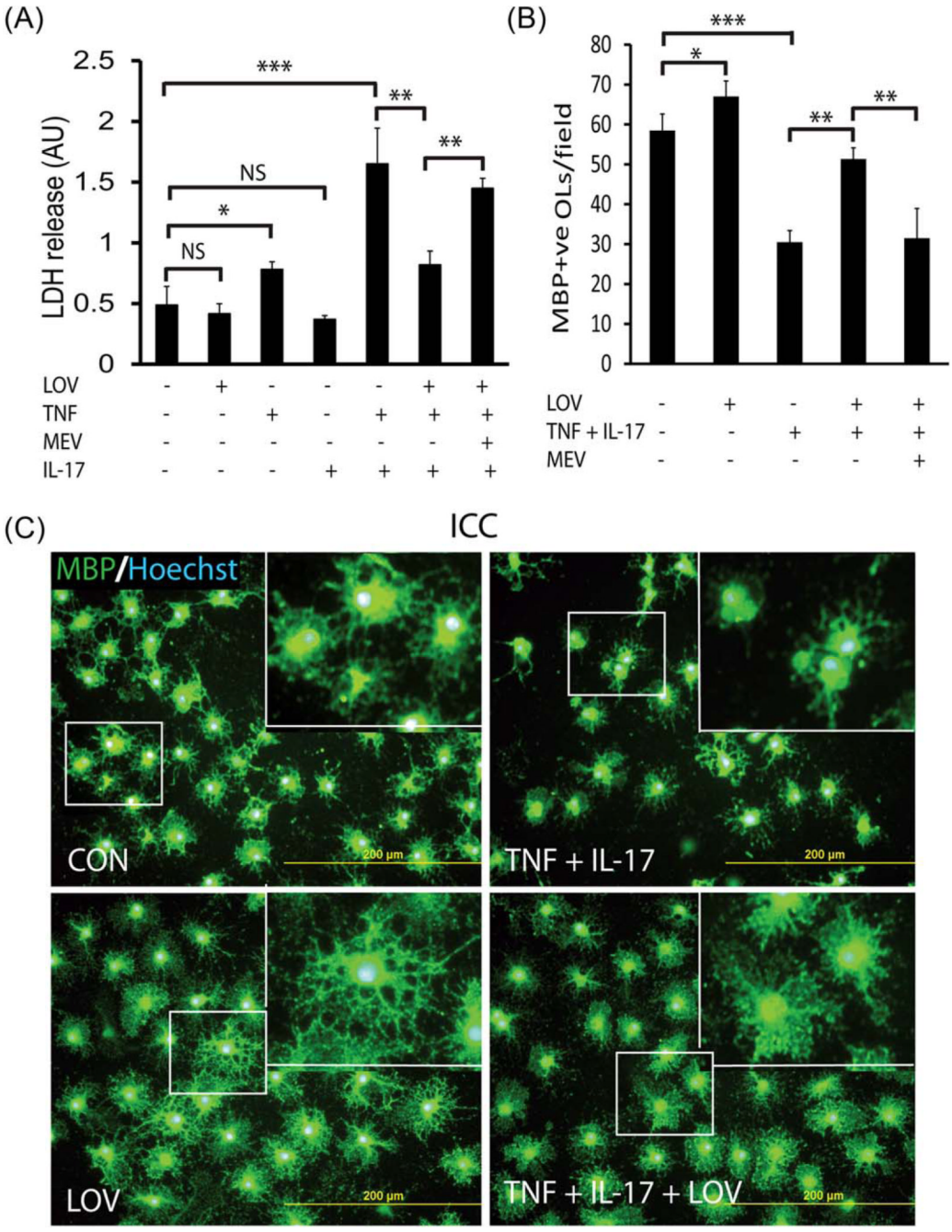

FIGURE 1.

LOV protects OLs from cytokine toxicity. OLs (2,000 cells/cm^2) were incubated with TNF-α (10 ng/mL) and IL-17 (25 ng/mL) in the presence or absence of LOV (2.0 μM)/or L-mevalonate (MEV; 100 μM). (**A**) The composite mean ± SE of three to four samples analyzed in triplicate depicts LDH release in the culture supernatants of treated OLs for 96 h. (**B**) The composite mean ± SE of similarly treated OLs on three to four slides depicts MBP^{+ve} OLs in 8–10 fields/slide. (**C**) The representative field of similarly treated OLs on slides depicts MBP^{+ve} OLs. Slides were counterstained with nuclear Hoechst dye. Inserts are the magnified region (square) in the representative field. Statistically significant as indicated: $^{*}P < 0.05$; $^{**}P < 0.01$; $^{***}P < 0.001$; NS, not significant; ICC,

immunocytochemistry; CON, control. [Color figure can be viewed in the online issue, which is available at wileyonlinelibrary.com.]

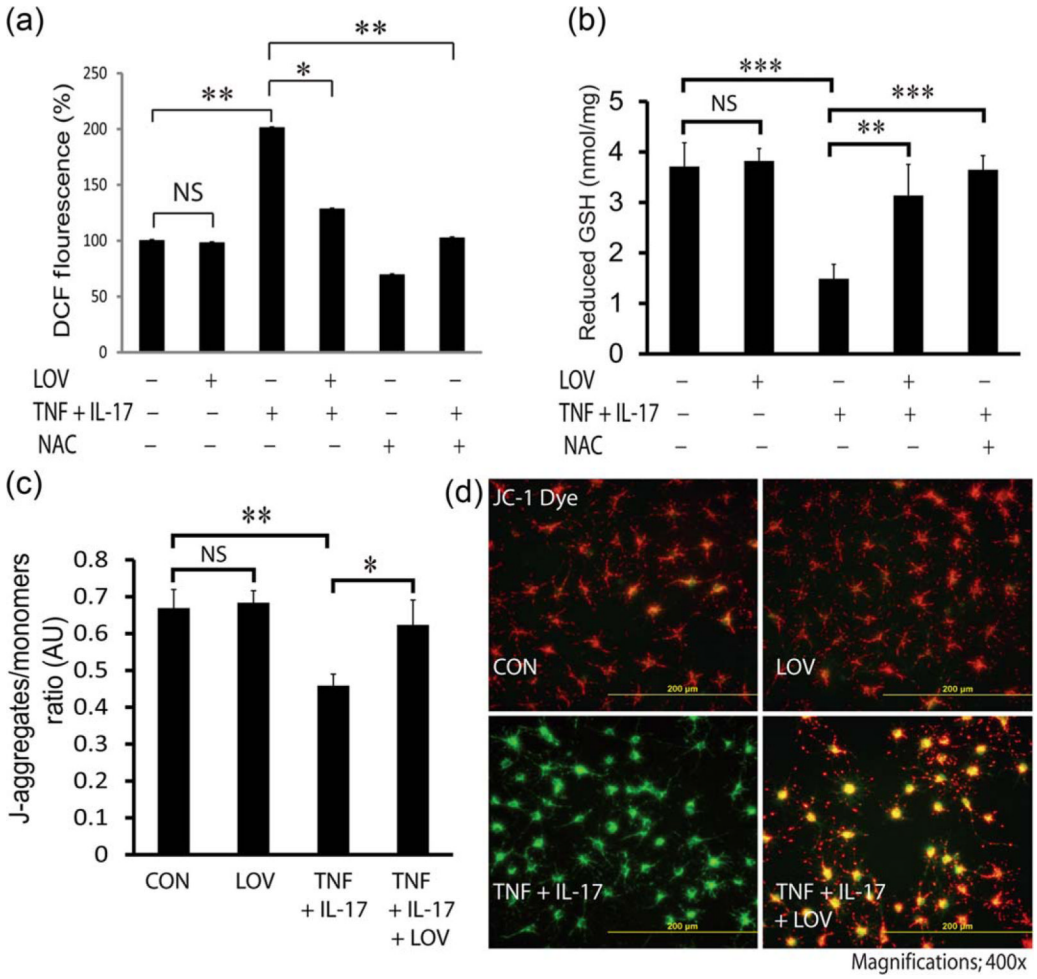

FIGURE 2.

LOV attenuates ROS generation and protects mitochondrial health in OLs exposed to cytokines. OLs were exposed to cytokines in the presence or absence of LOV (2.0 μM)/or *N*-acetyl cysteine (NAC; 5 mM) as detailed in the Fig. 1 legend. (**A**) The composite mean ± SE of three to four samples analyzed in triplicate depicts ROS levels in treated OLs for 48 h. Data are presented as changes % of controls. (**B**) The composite mean ± SE of three to four samples analyzed in triplicate depicts GSH (reduced) level in treated OLs for 48 h. (**C**) The composite mean ± SE of three to four samples analyzed in triplicate in treated OLs for 48 h depicting the ratio of J-aggregates/monomers (arbitrary units; AU). (**D**) The representative fields of slides depict a shift of fluorescence from orange red (mitochondrial membrane polarized) to green (mitochondrial membrane depolarized) in treated OLs for 48 h. Statistical significance as indicated in Fig. 1 legend. [Color figure can be viewed in the online issue, which is available at wileyonlinelibrary.com.]

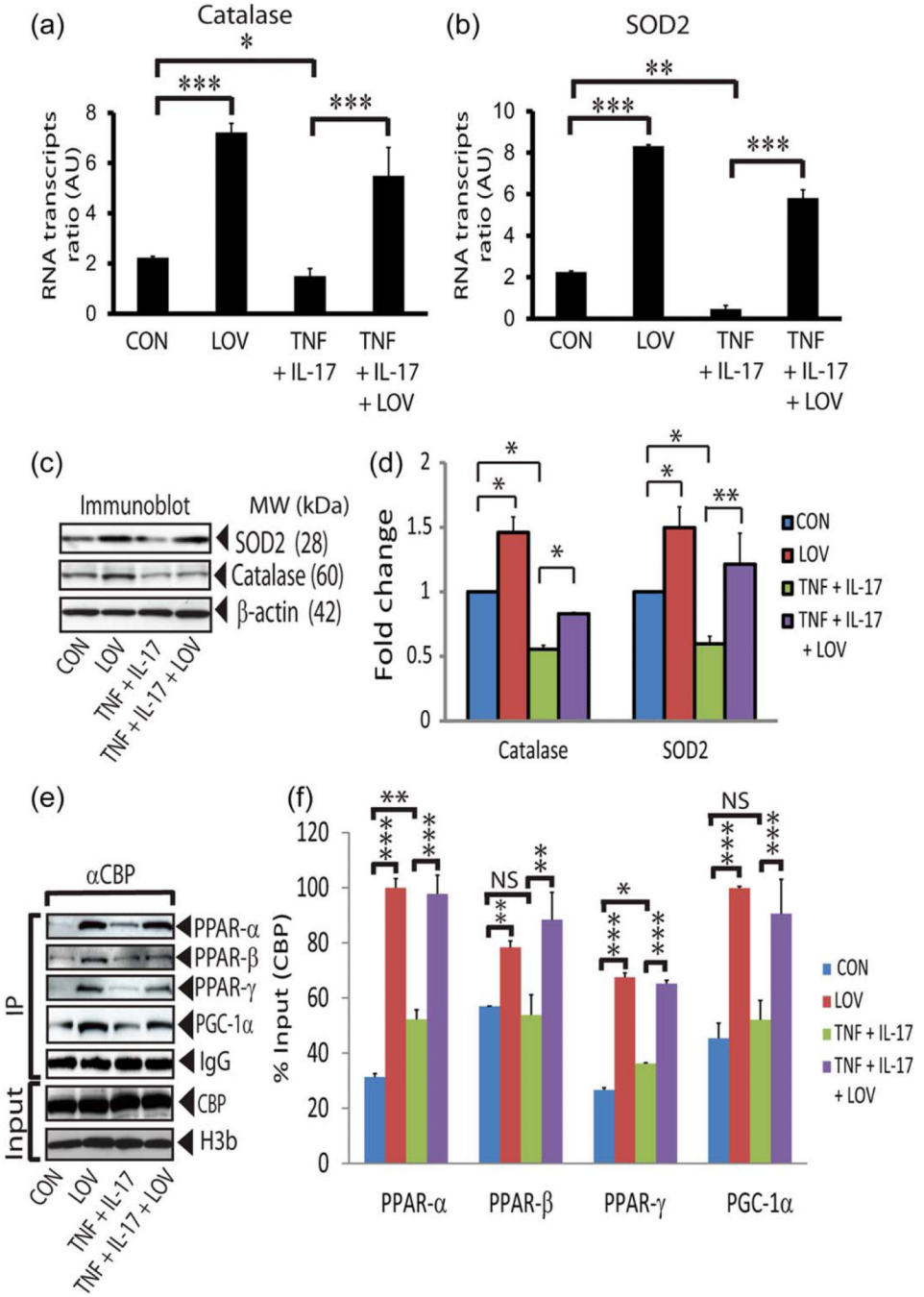

FIGURE 3.

LOV enhances ROS detoxifying defense in OLs exposed to cytokines. OLs were exposed to cytokines and LOV as detailed in the Fig. 1 legend for different durations. The composite mean ± SE of three to four samples analyzed in triplicate depicts levels of catalase (**A**) and SOD2 (**B**) mRNA transcripts in treated OLs for 24 h. Data is presented as the ratio to *β*-actin mRNA transcript level. Representative immunoblots (**C**) and the composite mean ± SE (**D**) of three to four samples depict levels of catalase and SOD2 protein normalized to *β*-actin protein level in treated OLs for 24 h. Representative immunoblots (**E**) and the composite mean ± SE (**F**) of three to four samples depict levels of the targeted proteins normalized to

CBP protein and presented as % input of protein analyzed by immunoprecipitation (IP) using anti-CBP antibodies in the nuclear fractions of treated OLs for 24 h. CBP and histone 3b (H3b) were used as gel loading controls. Statistical significance as indicated in Fig. 1 legend. [Color figure can be viewed in the online issue, which is available at wileyonlinelibrary.com.]

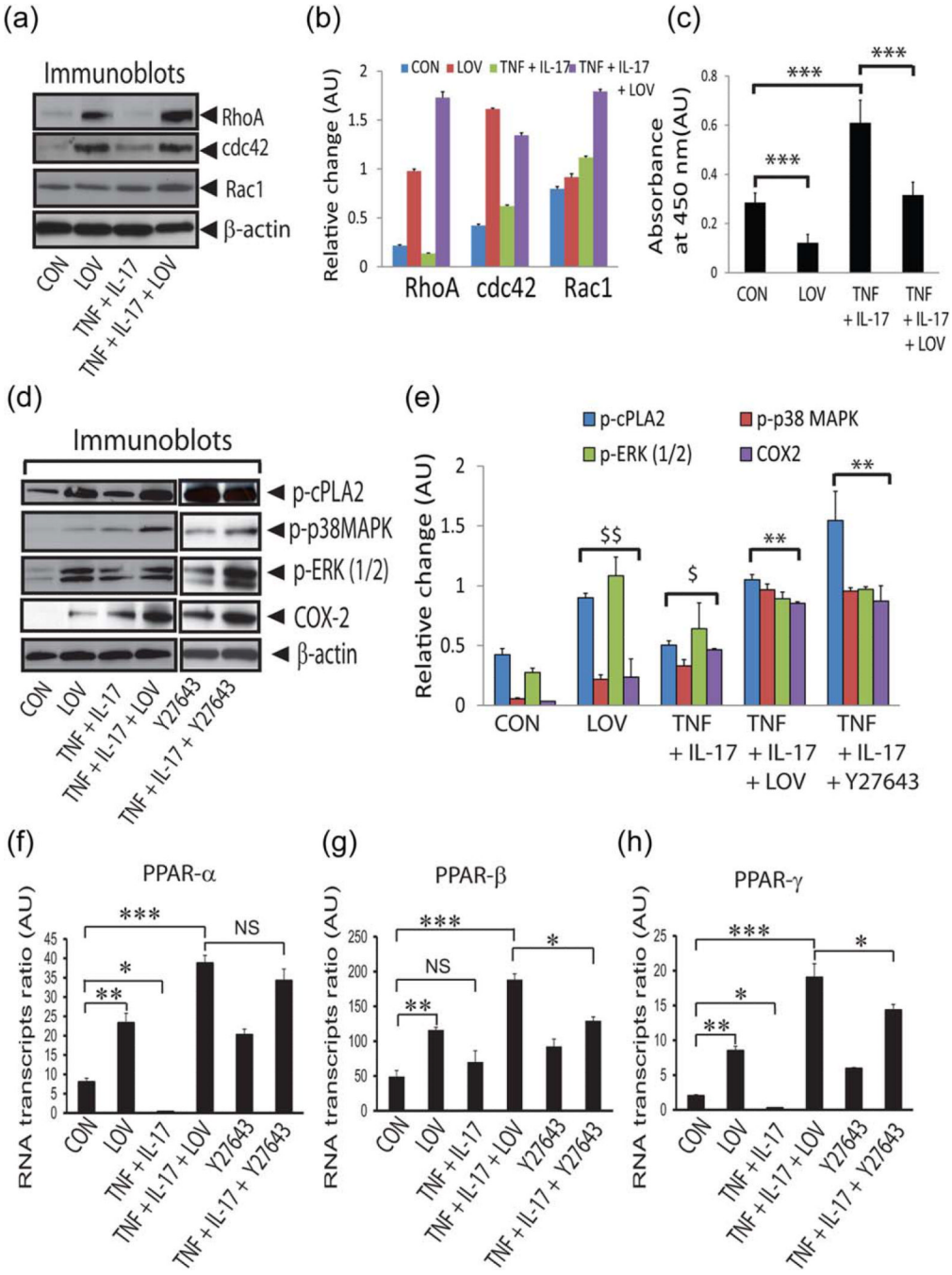

FIGURE 4.

LOV-mediated inhibition of Rho-ROCK activity enhances PPARs transactivation in OLs. OLs were exposed to cytokines and LOV as detailed in the Fig. 1 legend. Representative immunoblots (**A**) and the composite mean ± SE (**B**) of three samples depict levels of Rho family GTPases normalized to *β*-actin in the cytoplasm of treated OLs for 24 h. (**C**) The composite mean ± SE of similarly treated three samples depicts ROCK activity in the lysate (200 *μ*g of protein) of OLs. Representative immunoblots (**D**) and the composite mean ± SE (**E**) of three to four samples depict protein levels in treated OLs for 24 h. (**F–H**) The composite mean ± SE of three to four samples depicts PPAR subtype mRNA transcripts

normalized to β-actin in treated OLs for 24 h. Statistical significance as indicated in Fig. 1 legend. For E, \$$P < 0.05$ and \$\$$P < 0.01$ versus CON and $^{**}P < 0.01$ versus TNF + IL-17. [Color figure can be viewed in the online issue, which is available at wileyonlinelibrary.com.]

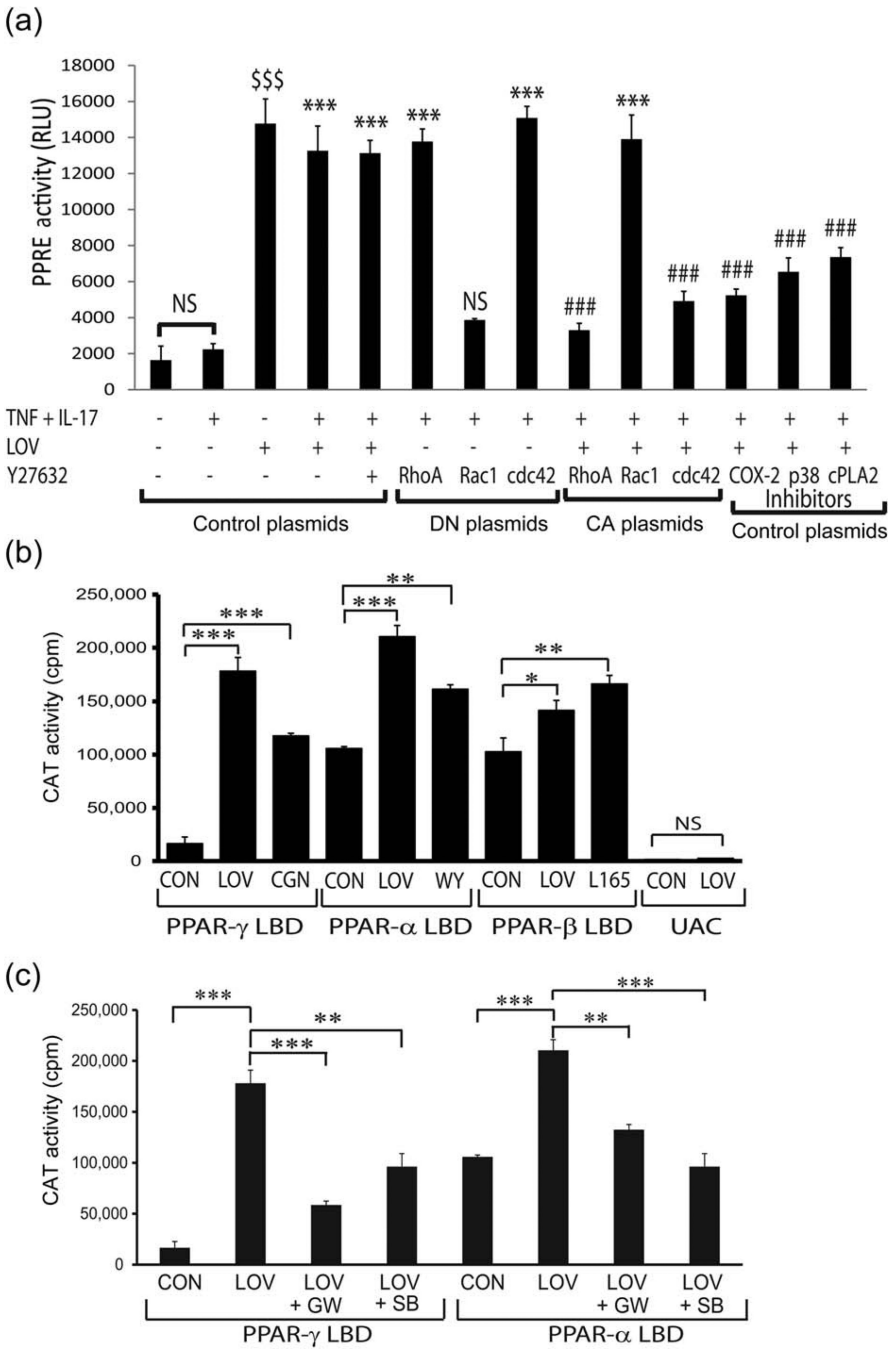

FIGURE 5.

LOV enhances PPARs transactivation in B12 cells via production of PPARs ligands. B12 cells (2,000 × cm^2) were treated with LOV (2.0 μM) or other pharmacological agents after transient transfection with the plasmids for PPRE and β-galactosidase activity or with PPAR-GAL4/$(UAS)_5$-CAT reporter system. (**A**) The composite mean ± SE of three to four samples analyzed in triplicate depicts PPRE reporter activity/β-galactosidase activity in treated B12 cells for 24 h after transfection with control/or DN/CA forms of the RhoA, cdc42, and Rac1 plasmids and/or treated with inhibitors of COX-2 (0.25 μM), p38 MAPK (SB203580; 2 μM), and cPAL2 (2 μM). (**B** and **C**) The composite mean ± SE of three to four samples analyzed in triplicate depict CAT reporter activity in treated B12 cells for 24 h.

Data are presented as counts per minute (cpm) normalized to β-galactosidase activity. Pharmacological agents were agonists of PPAR-γ (ciglitazone; 0.5 μM), PPAR-α (WY14643; 100 μM), and PPAR-β (L-165041; 20 nM) or inhibitors of PPARγ (GW9662; 0.25 μM), PPAR-α (GW6471; 0.1 μM), and p38 MAPK (SB203580; 2 μM). Statistical significance as indicated in Fig. 1 legend for B and C. For A, $^{***}P < 0.001$ and NS (not significant) versus TNF-α and IL-17; ###$P < 0.001$ versus TNF + IL-17 + LOV or Y27632 and \$\$\$$P < 0.001$ versus no treatment. RLU; relative light units.

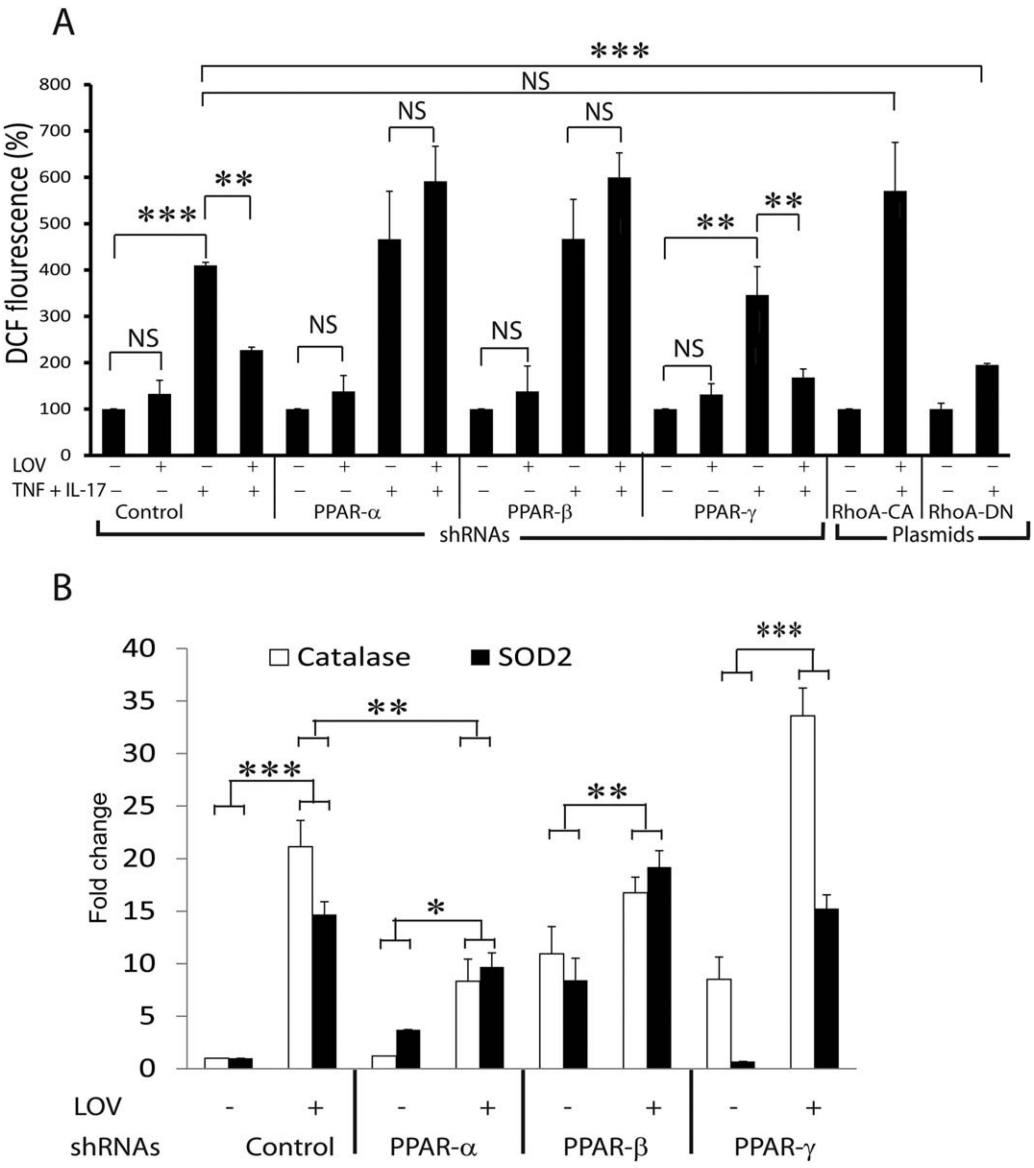

FIGURE 6.

PPARs depletion affects the attenuation of ROS generation and the expression of ROS detoxifying enzymes in LOV treated B12 cells. The expression of PPARs in B12 cells was reduced by transfection with single/or double PPAR subtypes shRNA plasmids. Likewise, RhoA expression was increased or reduced in B12 cells by transfection with RhoA-CA and RhoA-DN plasmids, respectively. (A) The composite mean ± SE of three to four samples analyzed in triplicate depicts a ROS level in B12 cells and treated with LOV or TNF plus IL-17 for 48 h. (B) The composite mean ± SE of the three samples analyzed in triplicate depicts catalase and SOD2 mRNA transcripts levels normalized to *β*-actin in treated B12 cells for 24 h. Statistical significance as indicated in Fig. 1 legend.

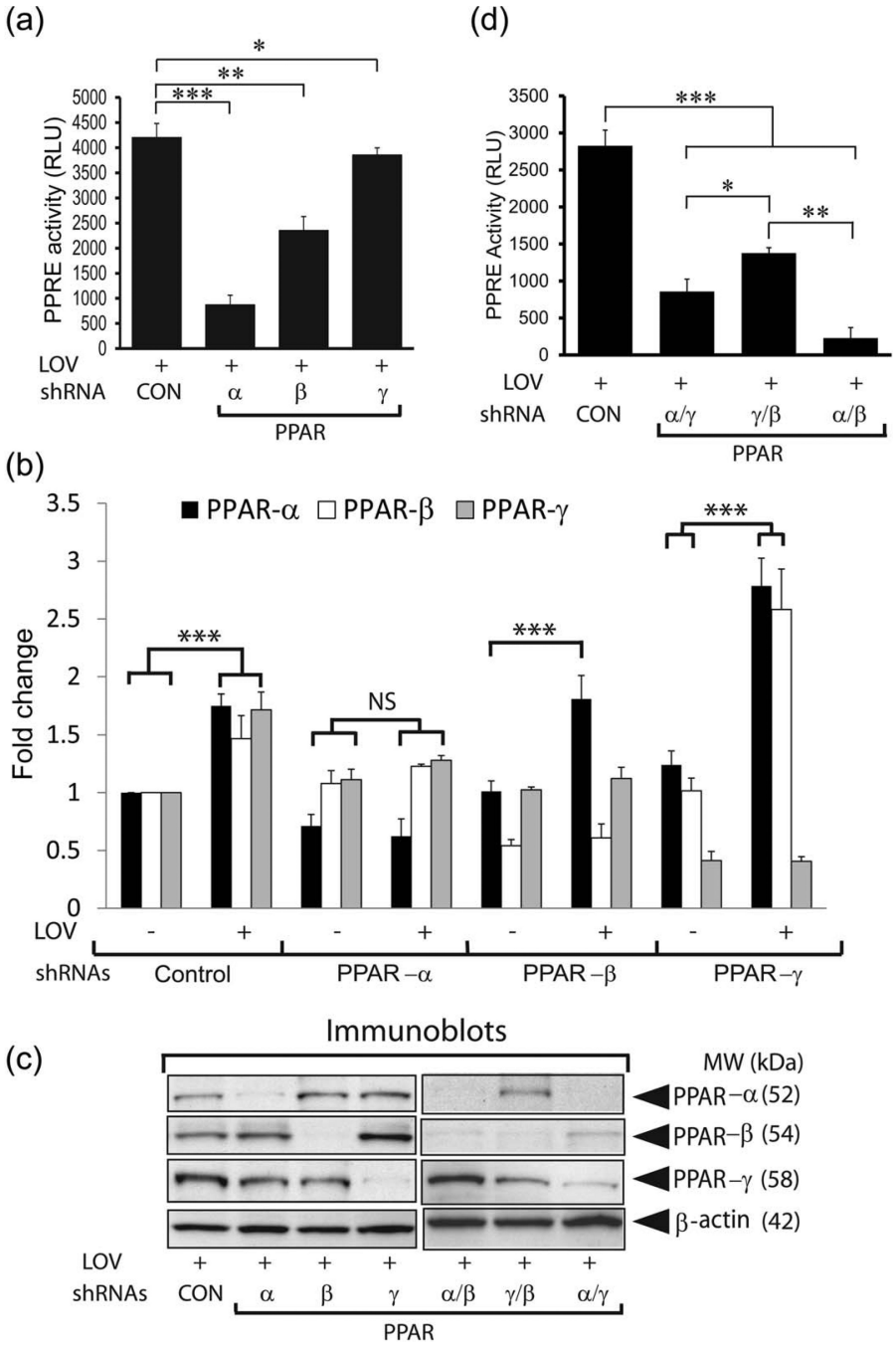

FIGURE 7.

PPAR depletion affects LOV-induced PPRE reporter activity in B12 cells. The knockdown of single/or double PPAR subtype expression in B12 cells was performed by using shRNA plasmids. (**A** and **D**) The composite mean ± SE of three to four samples analyzed in triplicate depicts PPRE reporter activity (RLU) in treated cells for 24 h. (**B**) The composite mean ± SE of three to four samples analyzed depicts PPAR subtype/*β*-actin mRNA transcripts ratio in treated B12 cells for 24 h. (**C**) Representative immunoblots (IB) depict PPAR protein levels in treated B12 cells for 24 h after transfection with single/or double PPAR subtype shRNA plasmids. Statistical significance as indicated in Fig. 1 legend.

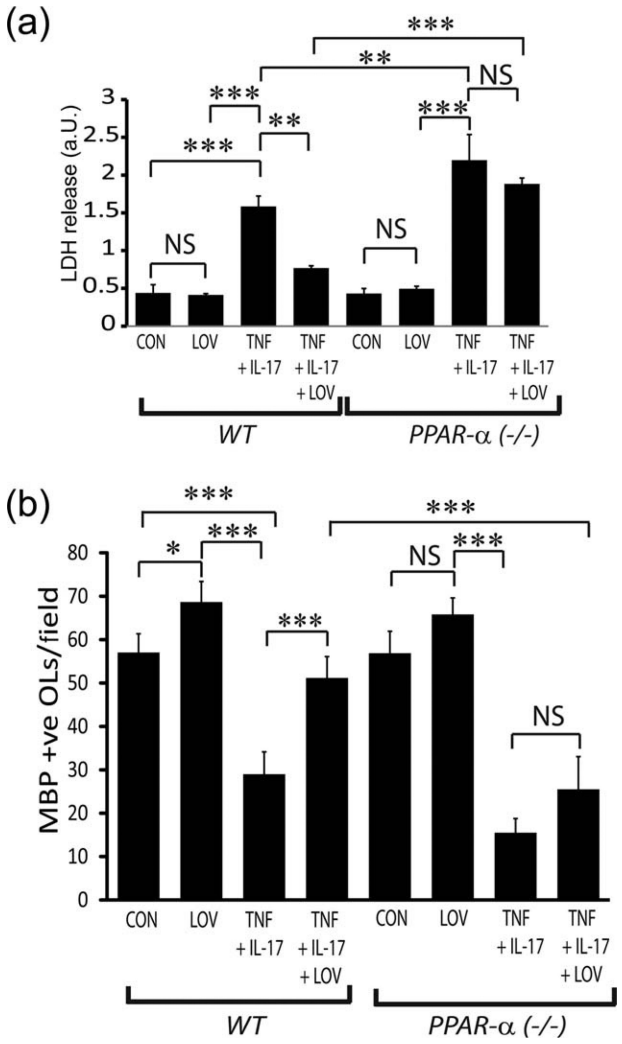

FIGURE 8.

LOV-mediated protective effects were lacking in PPAR-α-deficient OLs exposed to cytokines. OLs from wild type (WT) and PPAR-$\alpha^{(-/-)}$ mice were exposed to TNF plus IL-17 and LOV as detailed in the Fig. 1 legend. (**A**) The composite mean ± SE of three to four samples analyzed in triplicate depicts LDH release in the culture supernatants of treated OLs for 96 h. (**B**) The composite mean ± SE of three to four slides analyzed in triplicate depicts a MBP+ve OLs/field of the slide in treated OLs for 96 h. Statistical significance as indicated in Fig. 1 legend.

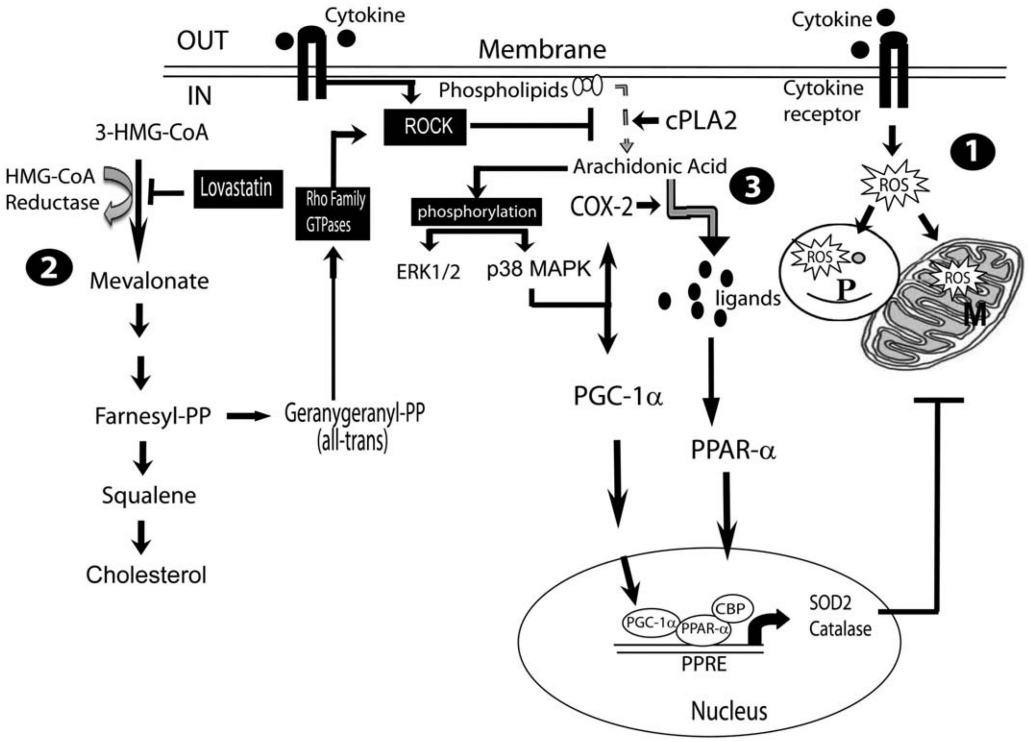

FIGURE 9.

Schematic diagram depicts the underlying mechanism by which LOV protects OLs from cytokine toxicity. **1**, TNF-α and IL-17-induced signaling mechanisms induce ROS generation thereby affecting peroxisome (P) and mitochondria (M) functions via activation of NADPH oxidase in OLs (Paintlia et al., 2011). **2**, LOV-mediated inhibition of mevalonate synthesis depletes the intracellular level of isoprenoids including geranylgeranyl-pyrophosphate (GGPP) leading to the inhibition of small Rho family GTPases, i.e., RhoA, cdc42, and Rac1 thus Rho-associated kinase (ROCK) activity in OLs. **3**, ROCK activity inhibition enhances cPLA2 phosphorylation that releases arachidonic acid from phospholipids (membrane), a substrate of COX-2 that produces PPARs ligands via activation of ERK (1/2) and p38 MAPK in OLs. P38 MAPK also induces PGC-1α transactivation that, in turn, enhances PPAR-α-dependent transcription of catalase and SOD2 genes in OLs.

TABLE 1

List of Primers Used for Quantitative Real-Time PCR Analysis

Gene name	Primer sequence
β-Actin	**FP:** 5'-agctgtgctatgttgccctagact-3'; **RP:** 5'-accgctcattgccgatagtgatga-3'
PPAR-α	**FP:** 5'-tcgggatgtcacacaatggaatcc-3'; **RP:** 5'-cgtgttcacaggtaaggatttctgcc-3'
PPAR-γ	**FP:** 5'-gcggaagccctttggtgactttat-3'; **RP:** 5'-tgggcggtctccactgagaattat-3'
PPAR-β	**FP:** 5'-tcatccacgacattgagacgctgt-3'; **RP:** 5'-cacatgcacgctgatctcgttgta-3'
Catalase	**FP:** 5'-gagaggaaacgcctgtgtgag-3'; **RP:** 5'-aagagcctggactcgggccc-3'
SOD2	**FP:** 5'-aaactgacagctgtgtctgtggga-3'; **RP:** 5'-gtactgatgctggctactgatg-3'

FP, forward primer

RP, reverse primer.